J Forensic Sci, January 2008, Vol. 53, No. 1
doi: 10.1111/j.1556-4029.2007.00606.x
Available online at: www.blackwell-synergy.com

TECHNICAL NOTE

Terry J. Henderson,[1] *Ph.D.; David B. Cullinan,*[2] *Ph.D.; Richard J. Lawrence,*[3] *M.A.; and Jonathan M. Oyler,*[1] *B.A.*

Positive Identification of the Principal Component of a White Powder as Scopolamine by Quantitative One-Dimensional and Two-Dimensional NMR Techniques

ABSTRACT: An unidentified white powder collected as evidence in an intelligence investigation was characterized exclusively by nuclear magnetic resonance (NMR) analysis. A small fraction of the powder dissolved in D_2O was subjected to a series of one- and two-dimensional techniques which were used to elucidate the molecular structure of the powder's major component and positively identify it as the scopolamine biotoxin. Quantitative one-dimensional experiments identified individual proton and carbon atom sites, and conventional ^{14}N spectroscopy detected a single nitrogen atom site. Heteronuclear single quantum coherence data correlated all protons to their directly bonded carbon atom, and together with the quantitative spectra, were used to determine the number of protons directly bonded to each carbon atom. The presence of a methyl, carboxyl, and a benzyl group was also identified from these data. Correlation spectroscopy detected a three proton and a nine proton $J_{H,H}$ network, representing a CH_2CH moiety and seven carbon atom ring, respectively. These five elements were assembled into an almost complete molecular structure by using long-range, *J*-coupled, ^1H–^{13}C pairs detected by heteronuclear multiple bond correlation (HMBC) spectroscopy and ^1H–^1H dipolar-coupled pairs found from nuclear Overhauser effect spectroscopy (NOESY) data. Additional oxygen atom sites were inferred from ^1H–^{13}C correlation intensities in the HMBC spectra along with ^1H and ^{13}C chemical shift values, or directly from NOESY correlations. Only a single oxygen atom site could not be inferred from NMR data, but its presence was inferred from comparisons to target analyte structures to complete the structure of the scopolamine molecule. To confirm these results, an ethanol/H_2O solution of the powder was analyzed by direct infusion into an ion trap mass spectrometer. A prominent base signal was observed at m/z 304.1 amu, corresponding to the protonated molecular ion of scopolamine. Subsequently, the ion was selected and subjected to collision-induced dissociation, producing characteristic major MS/MS fragments at m/z 138.1 and 156.1. Comparisons of ^1H and ^{13}C chemical shift values and $J_{H,H}$ values measured from our NMR data were found to agree very favorably with previously reported values for scopolamine in D_2O.

KEYWORDS: forensic sciences, molecular structure, biological toxins, tropane alkaloids, nuclear magnetic resonance, mass spectrometry

As demonstrated by the recent attacks involving ricin (1,2), biochemical weapons pose a threat not only to U.S. and Allied militaries but also to innocent civilians as well. The weapons are attractive to foreign states or terrorists seeking a mass-destruction capability, simply because they are relatively inexpensive to produce and do not require the elaborate technical infrastructure needed for nuclear weapons manufacturing. Biological toxins are poisonous compounds produced by different types of living organisms. Those that are highly toxic to humans and are stable, easily available and manageable, are important for the threat they present. Chemically, the toxins are peptides or proteins of various sizes, large glycoproteins, polysaccharides, or other organic compounds of different sizes and structures. Bacterial toxins are proteins that are a normal part of the metabolic machinery of the pathogen. Algal toxins are produced by many different algae, and constitute a very diverse group of compounds ranging from simple ammonia to complex polypeptides and polysaccharides. Dynoflagellates are a source of some potent, nonprotein toxins such as saxitoxin and tetrodotoxin; one such toxin is the cause of red tide. Mycotoxins comprise a wide variety of nonprotein chemical substances produced by molds and fungi. Specific parts of some plants contain toxins which are extremely poisonous. The glycoproteins ricin from castor beans and abrin from Abrus seeds are examples of these plant toxins. Finally, there are a number of toxins produced by animals, including the nonprotein batrachotoxin from the Columbian frog, and a variety of peptide and proteins from marine snails, scorpion venoms, and snake venoms.

Crimes and criminal actions involving biological toxins are explicitly described in Chapter 10 of Title 18 of the United States Code. In general, with the exception of certain representatives of the Federal Government, it is unlawful for anyone to develop, produce, acquire, stockpile, own, possess, use or threaten to use any biological toxin. This applies to all persons within the United States and U.S. Nationals in foreign countries. In addition, it is unlawful to use the toxins against a U.S. National outside of the United States, or while on any property that is owned, leased, or used by the United States or its Government, whether within or outside of the United States. Chapter 113B of the Title describes biological toxins as weapons of mass destruction, and the use of such weapons as acts of terrorism. Due to the September 2001 terrorist attacks in New York City and Washington, D.C., Chapters 10 and

[1]U.S. Army Edgewood Chemical Biological Center, AMSRD-ECB-RT-CF, E5100, 5183 Blackhawk Road, Aberdeen Proving Ground, MD 21010-5424.
[2]Science Applications International, Corp., Gunpowder Branch, PO Box 68, Aberdeen Proving Ground, MD 21010-0068.
[3]Battelle Eastern Science and Technology Center, Battelle Memorial Institute, 1204 Technology Drive, Aberdeen, MD 21001.

Received 4 Aug. 2006; and in revised form 11 April 2007; accepted 24 June 2007.

Journal compilation © 2008 American Academy of Forensic Sciences
No claim to original U.S. government works

113B were recently amended in House Resolution 3162, better known as the U.S.A. Patriot Act of 2001 (3). Many biological toxins are on the U.S. Munitions Import List defined in Title 27, Part 47 of the U.S. Code of Federal Regulations (27 CFR 47), and therefore, their importation into the United States is unlawful for all individuals except those registered by the Director of the Department of Alcohol, Tobacco and Firearms.

Evidence from the scene of a terrorist or military attack suspected to involve a biotoxin weapon is usually taken to a forensic laboratory licensed to handle chemical warfare agents and biochemical weapons. The single, most important determination that the laboratory must make is whether the sample contains toxic substances, particularly in the form of the weapons themselves, their degradation products, or impurities from their preparation. This information is important not only for legal evidence, but determines the sample's potential to harm laboratory personnel, and how the sample is to be handled during analysis. The strongest evidence for the presence of any toxic compound is its detection by chemical analysis together with a complete elucidation and conformation of its molecular structure. In the simplest cases, investigating officials have an idea of the chemical or biochemical weapon used from evidence collected at the scene of the attack, and the list of potential target analytes is small. Routine analytical techniques such as gas chromatography/mass spectrometry can be used to identify the weapon and verify its molecular structure. Evidence for the use of chemical or biotoxin weapons, however, is not always available. For example, the use of a biological weapon may only be surmised from symptoms exhibited by people at the scene of the attack, and the use of toxic industrial chemicals or other toxic materials cannot be ruled out. The list of potential target analytes and analytical methods required to evaluate samples, therefore, can grow very large. To complicate matters, after determining that a sample does not contain toxic or hazardous materials, criminal investigators may decide to characterize its chemical composition completely, further increasing the size of the potential target analyte list. In these cases, forensics laboratories turn to spectrometric techniques, like nuclear magnetic resonance (NMR) spectroscopy, to elucidate the molecular structure of the chemical components. Although more expensive and less sensitive than conventional techniques, NMR spectroscopy does not require extensive sample preparation, and generates results that are easily interpreted.

We have recently performed a complete structural determination in an effort to characterize a forensic sample. Approximately 50 g of a white powder seized in an intelligence investigation were brought to our laboratory for chemical weapons screening. After testing negative for the suspected chemical weapons and their degradation products, the sample was analyzed further to identify its chemical composition. Relying heavily on two-dimensional NMR spectroscopy, the analysis positively identified the powder as the biological toxin scopolamine, a powerful antagonist of acetylcholine which is known to act at the autonomic parasympathetic postganglionic junction. Direct infusion positive electrospray ionization ion trap mass spectrometry (ESI^+-MS) was used as a complementary technique to confirm the NMR results. We present the details of this characterization and structural elucidation herein.

Experimental Protocols

Chemicals, Solvents, and Supplies

D_2O and $CDCl_3$ (both at ≥99% isotope enrichment), as well as the chemical shift reference compounds tetramethylsilane and the sodium salt of 3-(trimethylsilyl)-1-propane-sulfonic acid, were purchased from Sigma-Aldrich (St. Louis, MO). High-performance liquid chromatography (HPLC) grade ethanol and H_2O, and (−)-scopolamine hydrochloride were also purchased from Sigma-Aldrich. All NMR sample tubes were purchased from Wilmad-Labglass (Buena, NJ).

Sample Preparation

Samples were prepared as concentrated solutions in deuterated solvents for NMR spectroscopy. Approximately 56 mg of an unidentified white powder was dissolved in 1.25 mL D_2O, and determined to have a pD of 6.0 as described (4). A second solution was prepared in $CDCl_3$ at a concentration of *ca.* 20 mg/mL. Samples were placed into separate 5-mm NMR sample tubes just prior to NMR analysis. For mass spectrometric analyses, 1 mg of the powder was dissolved in 1 mL of 50% ethanol/50% H_2O (v/v) to give a 1 mg/mL stock solution. A 1:10 dilution of this stock with the same ethanol/H_2O solution was analyzed directly by ESI^+-MS and ESI^+-MS/MS.

NMR Spectroscopy

All NMR spectroscopy was conducted at 11.75 Tesla, using an Avance DRX-500 spectrometer (Bruker-Biospin Corp., Billerica, MA) with XWIN-NMR software (version 3.1) for data acquisition and processing. The spectrometer was fitted with a triple resonance TXI probehead (Bruker-Biospin Corp.) having dedicated ^1H, ^{13}C and ^{31}P channels (inverse-detection configuration) and actively shielded *x*-, *y*- and *z*-gradient coils. A three-channel, 10-ampere Acustar II 3 × 10 gradient amplifier (Bruker-Biospin Corp.) was used to amplify gradient coil pulses, with all pulse timing controlled from the spectrometer pulse programs. Experiments were conducted at 25.0 ± 0.2°C unless noted otherwise, with the sample spinning at 20 Hz for one-dimensional experiments only. For two-dimensional spectroscopy, quadrature detection was used exclusively for collecting complex data in the direct dimension (t_2), while various phase cycling schemes used for the indirect dimension (t_1) gave either real or complex data. Both ^1H and ^{13}C chemical shifts were referenced to internal tetramethylsilane, or 3-(trimethylsilyl)-1-propane-sulfonic acid in the case of aqueous solutions.

Quantitative NMR Spectroscopy—All one-dimensional spectroscopy was conducted under quantitative conditions to determine the exact number of nuclei represented for each signal, imposing the need to evaluate spin-lattice relaxation time (T_1) values for all signals in the spectra. For both ^1H and ^{13}C spectroscopy, T_1 values were estimated from signal intensities in data sets using the inversion recovery pulse sequence [180°-τ-90°-acquisition] and a single exponential expression for T_1 (5). ^1H data sets were recorded with relaxation delays ≥$5T_1$ for the slowest relaxing signal in the spectra, ensuring quantitative recovery of all signals between successive pulses. ^{13}C data sets derived from experiments using relaxation delays ≥$8T_1$ the slowest relaxing ^{13}C signal in the spectra (*ca.* 20 s) to ensure the complete elimination of nuclear Overhauser effect (NOE) enhancements (6). Signal intensities were determined by electronic integration of expanded regions around the signals. Spectral regions chosen for integration included all spinning sideband and ^{13}C satellite signals originating from the parent signal.

^1H free induction decay data containing of 16,384 or 65,536 complex points were recorded from the summation of 32 acquisitions using 10–12 ppm spectral windows, 90° pulse widths of

8.5 μsec, and relaxation delays between 5 and 9 s. These data were Fourier transformed directly into spectra and manually adjusted into pure absorption mode.

All $^{13}C\{^1H\}$ data sets were recorded with 65,536 complex points, using 90° pulse widths of 11.3 μs, 220 ppm spectral windows, 20 s relaxation delays and inverse-gated ^1H decoupling (decoupling during data acquisition only) with a low-power, composite pulse sequence (7). Alternatively, quantitative $^{13}C\{^1H\}$ Distortionless Enhancement by Polarization Transfer (DEPT) data sets were recorded using the sensitivity-enhanced Q-DEPT pulse sequence (8). Recorded data sets were multiplied by an exponential window function (apodized) with a line-broadening factor of 2 Hz before Fourier transformation into spectra and manual phase correction into pure absorption mode.

^1H–^1H Correlation Spectroscopy—*J*-coupled ^1H pairs were identified with a pulsed-field gradient, double-quantum filtered, correlation spectroscopy (COSY) pulse sequence (XWIN-NMR program "cosygpmftp") using time proportional phase incrementation (TPPI) phase cycling (9) for quadrature detection in the indirect dimension. The data set contained 4096 free induction decays, each with 8192 complex points from two data accumulations using 1 s relaxation delays to give a final 4096 real × 8192 complex ($t_1 \times t_2$) data matrix. Spectral windows of 6.4 ppm were used in both dimensions, resulting in a total acquisition time of 5 h 42 min. The t_2 free-induction decay data were zero-filled to 16,384 complex points, then apodized with a line-broadening factor of 0.5 Hz before Fourier transformation. The resulting t_1 free induction decay data were zero-filled to 8192 real points, apodized with a 1.5 Hz line-broadening factor, and finally Fourier transformed into a spectrum of 8192 × 8192 ($f_1 \times f_2$) real points.

Dipolar-coupled ^1H pairs were found with a nuclear Overhauser effect spectroscopy (NOESY) (10) sequence (XWIN-NMR program "noesygpst") incorporating gradient pulses during the mixing time (11) and a States-TPPI scheme to achieve quadrature detection in the indirect dimension (12). Data sets were recorded as a 512 × 2048 complex matrix using 6.6-ppm spectral windows in both dimensions. Each t_2 free induction decay resulted from eight data acquisitions using 4 s relaxation delays and 700 ms mixing times, giving a total acquisition time of 5 h 47 min. The t_2 data were multiplied by a sine window function before Fourier transformation. The resulting t_1 data were extended to 2048 complex points with a linear prediction algorithm (13–15), multiplied by a sine window function, and finally Fourier transformed into a spectrum containing 1024 real data points in both dimensions.

^1H–^{13}C Correlation Spectroscopy—One-bond, ^1H-^{13}C correlations were determined with a heteronuclear single quantum coherence (HSQC) pulse sequence (XWIN-NMR program "invietgssi") using a pulsed-field gradient echo/antiecho-TPPI gradient scheme (16–18). A 1024 × 8192 complex data matrix was collected with six ^1H acquisitions per t_1 increment using 2 s relaxation delays. The spectral widths were 6.4 and 220 ppm in the ^1H and ^{13}C dimensions, respectively, resulting in a total acquisition time of 5 h 45 min. ^1H data were apodized with a 4 Hz line-broadening factor before Fourier transformation. For t_1, data points were extended to 4096 complex points by linear prediction before multiplication with a sine-squared window function and final Fourier transformation into a 2048 × 4096 real spectrum.

Long-range, ^1H–^{13}C correlations were identified with a heteronuclear multiple bond correlation (HMBC) pulse sequence (XWIN-NMR program "inv4gplplrndqf") incorporating pulsed-field gradients for phase coherence selection and a low-pass *J*-filter to suppress one-bond correlations (19). Data were collected as a 512 real × 8192 complex matrix from 32 ^1H acquisitions per t_1 increment, each using 2 s relaxation delays. The spectral windows were identical to those in the HSQC experiment, and gave a total acquisition time of 15 h 1 min. ^1H data were multiplied by a trapezoidal window function before Fourier transformation to increase spectral resolution. ^{13}C data were extended to 1024 real points by linear prediction before multiplication by a sine squared window function and Fourier transformation into a 1024 × 4096 real spectrum.

Diffusion Oriented Spectroscopy—Data sets for diffusion ordered spectroscopy (DOSY) spectra were acquired with the longitudinal eddy current delay pulse sequence of Gibbs and Johnson (20), which incorporates a delay at the end of the experiment for avoiding spectral artifacts from residual eddy currents. For our spectrometer and probehead, the optimum value of the eddy current delay was found to be 5.0 ms. In addition, a presaturation pulse was incorporated into the pulse program (XWIN-NMR program "ledbpgp2s") to attenuate the solvent signal and increase analyte sensitivity. The experiments also incorporated 50-ms diffusion time delays and either 1.2 or 1.5-ms gradient pulses for recording data sets at 25 or 37°C, respectively. ^1H data sets acquired with 10 ppm spectral windows, 90° pulse widths and 6 s relaxation delays were recorded onto computer disk; total acquisition times were <30 min. The recorded data sets were multiplied by an exponential window function with a line-broadening factor of 1 Hz before Fourier transformation into spectra and manual adjustment into pure absorption mode. For each diffusion measurement, spectra from 16 separate data sets were collected as a function of gradient amplitude ranging between 2 and 95%.

Mass Spectrometry

Following NMR characterization, ESI^+-MS was performed on the sample with a Finnigan LCQ DECA ion-trap mass spectrometer (Thermoquest/Finnigan Corp., San Jose, CA), using a spray potential of 5 kV and a constant capillary temperature of 250°C. The 0.1 mg/mL sample solution was directly infused for *ca.* 1 min at 3 μL/min, and averaged spectra were collected. Initially, spectra were collected in full scan mode (mass range 35–1000 amu), and a prominent base peak at m/z 304.1 was observed. Subsequently, the mass spectrometer was operated in zoom scan centered on 300 ± 50 amu to identify the scopolamine molecular ion $(M+H)^+$. In product-ion scan mode, the m/z 304.1 ion was collected and subjected to 26% relative collision energy using nitrogen as a collision gas. Collision-induced dissociation produced major fragment ions at m/z 138.1 and 156.1.

Results and Discussion

NMR Identification and ESI^+-MS Conformation of Scopolamine

An unidentified white powder seized in an intelligence investigation was brought to our laboratory for detailed chemical analysis. Preliminary tests found that the powder did not contain chemical warfare agents (particularly the nerve agent VX or sulfur mustard blister agents) or their degradation products as initially suspected. The powder was then subjected to an extensive NMR analysis to characterize its principal components. A flowchart illustrating the order in which the NMR experiments were performed, and the conclusions deriving from them, is presented in Fig. 1.

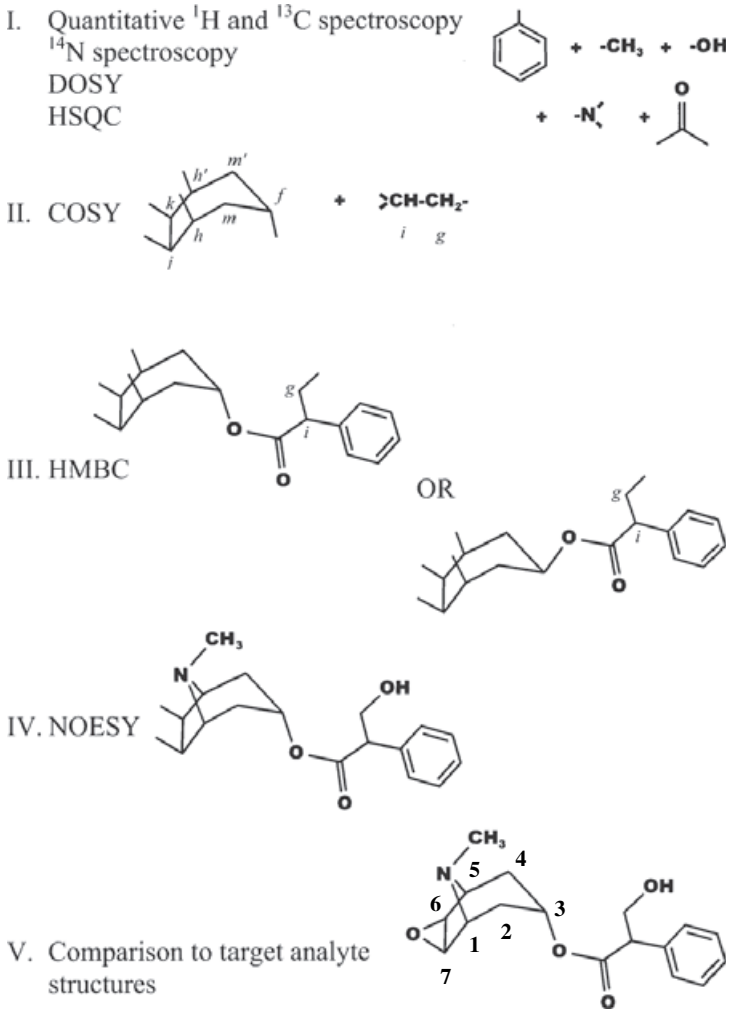

FIG. 1—*Summary of experiments used to analyze the unidentified powder dissolved in D_2O, and the structural information derived from each. Italicized letters designating individual carbon sites derive from Fig. 2, with primed (′) and unprimed pairs of letters representing different sites on the ring system correlating to the same ^{13}C signal. Tropane ring positions are numbered in the bottom panel.*

Solubility tests at room temperature found that the powder was freely soluble in H_2O, $CHCl_3$, ethanol and acetone, and because the H_2O signal did not appear to obscure ^{1}H analyte signals, the powder was dissolved directly into D_2O for NMR analysis. A quantitative $^{13}C\{^{1}H\}$ spectrum of this sample is presented in Fig. 2, where the signals are lettered in order of decreasing chemical shift, and a quantitative ^{1}H spectrum is shown in Fig. 3. Carbon atoms were correlated to their directly bonded protons using the HSQC spectrum shown in Fig. 4, and the information has been appended onto Fig. 3.

The quantitative spectra were examined first to determine the exact number of compounds comprising the powder and as much information relating to their structural formulas as possible. Integration of the ^{1}H signals revealed 20 unique ^{1}H sites in addition to that for the solvent. DOSY analysis revealed that all analyte protons had identical diffusion rates at both 25 and 37°C (not shown), demonstrating conclusively that they all reside on the same molecule. The ^{13}C spectrum revealed 17 novel carbon atom sites with 15 representing carbon atoms directly bonded to protons identified in the ^{1}H spectrum (see Fig. 4). We assumed that the remaining two ^{13}C signals also represented carbon atoms of the same molecule, as their measured integral values were virtually identical to those of many of the other carbon atoms. Signals were not detected with conventional ^{19}F and ^{31}P analyses, and ^{14}N spectroscopy revealed a single signal at 373 ppm (not shown). Finally, a quantitative ^{1}H spectrum of the powder dissolved in $CDCl_3$ contained an additional signal at 12.7 ppm (not shown), most likely from a single hydroxyl group proton. This observation, along with the single ^{13}C signal indicative of a carbonyl carbon atom (*a* in Fig. 2), implies that the analyte molecule contains at least two oxygen atoms.

The number of protons directly bonded to each carbon atom was determined by evaluating the quantitative spectra together with the HSQC correlations, leading to the identification of additional structural features. Four signals in the aromatic region of the ^{13}C spectrum (*b*, *c*, *d*, and *e* in Fig. 2) arise from six carbon atoms, and therefore, are indicative of a single benzyl group. This conclusion is corroborated by the HSQC data, which correlate three of these signals to others occurring within the aromatic region of the ^{1}H spectrum (*c, d*, and *e* in Figs. 3 and 4). The ^{1}H spectrum further illustrates that these signals represent five protons, all of which appear to be intimately *J*-coupled to one another. In another region of the ^{13}C spectrum, a single carbon atom appears to be bound directly to three, magnetically equivalent protons (*l* in Fig. 4), clearly representing a single methyl group.

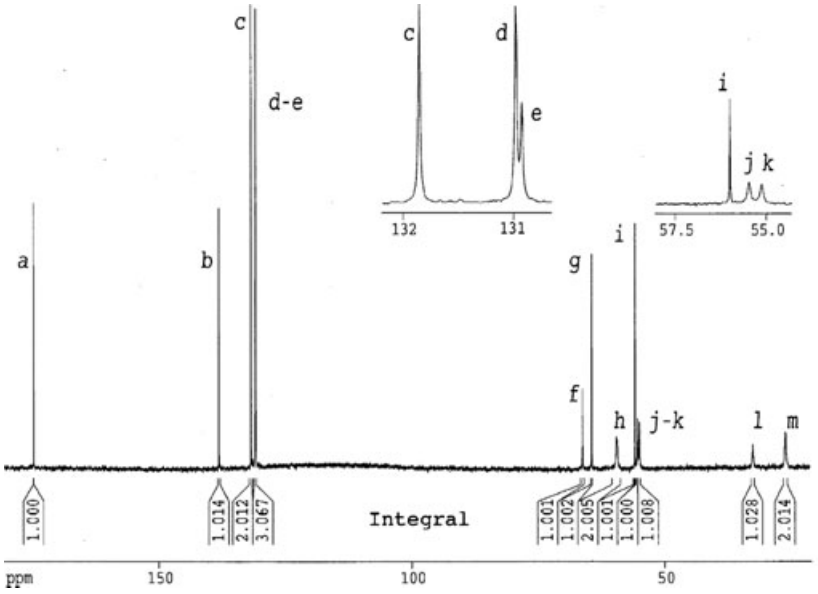

FIG. 2—*$^{13}C\{^{1}H\}$ spectrum of the unidentified powder dissolved in D_2O acquired under quantitative conditions. Signals are lettered in order of chemical shift (increasing resonance frequency), and their relative integral values are included. Insets show details of overlapping signals.*

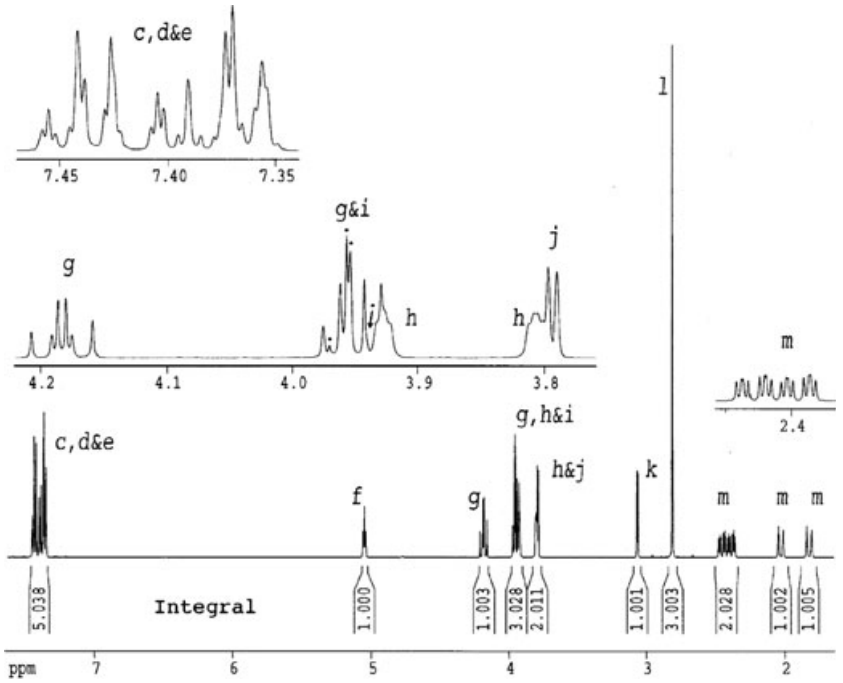

FIG. 3—*Quantitative ^{1}H spectrum of the unidentified powder dissolved in D_2O, with relative integral values shown for all signals. The HOD signal (4.8 ppm) was virtually eliminated by use of a presaturation pulse. Letters assigned to signals relate their protons to the signal for their directly bonded carbon atom (Fig. 2), determined from heteronuclear single quantum coherence spectroscopy (Fig. 4). Insets reveal details of complex spectral features, with solid circles designating the individual resonances for signal i.*

The remaining structural features were inferred from $J_{H,H}$ networks revealed by the COSY spectrum in Fig. 5. Two completely isolated coupling networks are apparent in addition to that of the benzyl group: a three-proton network (*g*–*g* and *g*–*i*), and a much more extensive, nine-proton network. Careful examination of the correlations demonstrates that the latter arises from a ring system of seven carbon atoms (see the arrows in Fig. 5). Starting with the autocorrelation for proton *f* (*f*–*f*), three correlations (*f*–*m*, *m*–*h*, and *h*–*j*) define an unbranched, aliphatic chain of four carbon atoms. Another set of correlations (*f*–*m*′, *m*′–*h*′ and *h*′–*k*) reveals a similar chain also starting with proton *f*, and a final correlation (*j*–*k*) connects the ends of these chains to close the ring. Strong coupling is evident between four of the ring system protons (δ_H = 1.75–2.55 ppm), all of which are correlated to the same ^{13}C signal by HSQC spectroscopy (*m* in Fig. 4). It is apparent that these protons are the axial-equatorial pairs for carbon atoms *m* and *m*′ on the ring (see Fig. 1). In the case of cyclohexane rings, equatorial proton signals are consistently found downfield (higher δ_H value) from those

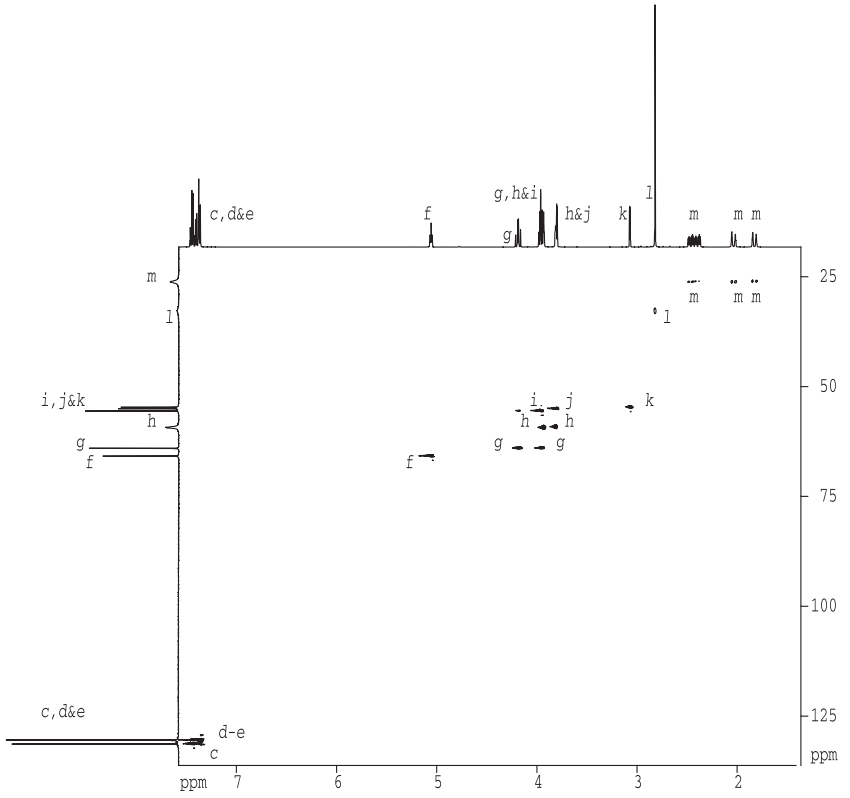

FIG. 4—*^{1}H–^{13}C heteronuclear single quantum coherence spectrum of the unidentified powder dissolved in D_2O, with the corresponding one-dimensional subspectra included for both dimensions. The lettering scheme is from Fig. 2.*

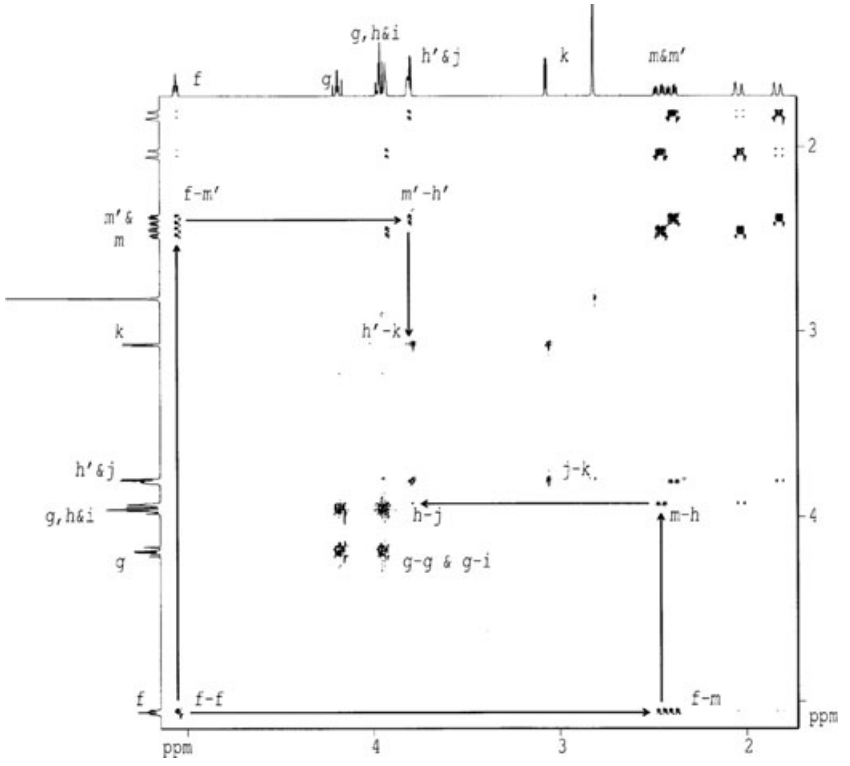

FIG. 5—*Correlation spectroscopy (COSY) subspectrum of the unidentified powder dissolved in D_2O, with the corresponding region of the ^{1}H spectrum shown for both dimensions. Correlations from a three-proton (g–g* and *g–i) and a nine-proton (f–m, m–h, h–j, f–m′, m′–h′, h′–k, and j–k)* $J_{H,H}$ *network are designated. Arrows illustrate the* $J_{H,H}$ *connectivity for the latter network, defining a seven carbon atom ring system. All lettering is consistent with Figs. 1 and 3.*

of the axial protons bonded to the same carbon atom (21), and we assigned signals to the protons accordingly (see Fig. 7 for assignments). In the three-proton network, the protons all correlate to one of two carbon atoms (*i* and *g* in Fig. 4, referred to as C*i* and C*g*, respectively), clearly the consequence of a CH_2 and CH group directly bonded to one another. Moreover, because C*i* and C*g* chemical shifts are far from the alkene region (δ_C = 80–160 ppm), this bond must be a single, rather than a double bond (see Fig. 1).

Long-range, ^1H–^{13}C correlations were identified by HMBC spectroscopy and were used to assemble the identified structural elements into a molecular structure. The experiment incorporates a specific delay for the evolution of long-range scalar couplings, and the detected correlations are a direct function of the delay. In the particular case of hydrocarbons, a relationship between $^3J_{CH}$ values and H–C–C dihedral angles has been suggested (22) which can be used to derive a delay time. A region of the HMBC spectrum displaying all relevant correlations is shown in Fig. 6. Long-range correlations were found between the aromatic protons H*ar* and the carbonyl carbon atom (C*a*–H*ar*), as well as carbon atom C*i* (C*i*–H*ar*). The substantially larger intensity of C*i*–H*ar* suggests that the benzyl group is directly bonded to C*i*, however, the detection of C*a*–H*ar* demonstrates that C*a* must also be in close proximity to the benzyl group. In addition to C*a*–H*ar*, four other C*a* correlations to remote protons are observed: C*a*–H*f*, two C*a*–H*g* correlations, and C*a*–H*i*. These can be rationalized by placing the carbonyl carbon atom between C*f* on the ring system and the CH_2CH moiety. We assigned a single bond between C*a* and C*i* because its corresponding correlation is significantly more intense than all other C*a* correlations with remote protons. Furthermore, the C*a*–H*ar* correlation is more likely a consequence of this bond rather than one between C*a* and C*g*, since the latter requires the unlikely detection of a five-bond correlation. For the connectivity between C*a* and C*f*, the much lower intensity of the C*a*–H*f* correlation relative the C*a*–H*i* and C*a*–H*g* intensities suggests that the two carbon atoms are not directly bonded, but that another atom occurs between them. We tentatively assigned an oxygen atom to be bound to both C*a* and C*f*, because all ^{13}C signals have already been assigned to structural elements, and the chemical shifts of the H*f* and C*f* signals are more indicative of an oxygen atom at this site rather than a nitrogen atom. The absolute configuration about C*f* cannot be surmised from the COSY, HSQC, or HMBC data, and therefore, both axial and equatorial C*f*–O bonds are possible (see Fig. 1).

Our final experimental effort relied on NOESY to place the nitrogen atom, the methyl group and the hydroxyl group within the conformational space around the two ring systems to infer their connectivities to specific atoms of the analyte molecule. The region of the NOESY spectrum illustrating key correlations is shown in Fig. 7. For the methyl protons (H*l*), strong correlations with the protons of C*h*, C*h′*, C*m*, and C*m′* [labeled respectively as *l*–*h*, *l*–*h′*, *l*–*m*(eq), and *l*–*m′*(eq)], all with very similar intensities, suggest that the methyl group occurs at a position equidistant from the four carbon atoms. Moreover, because the *l*–*m* and *l*–*m′* correlations involve the equatorial rather than axial protons, the methyl group must occur on the same side of the seven carbon atom ring system as the equatorial protons. The observations can be explained by connecting the nitrogen atom to both C*h* and C*h′*, and in turn, connecting the methyl group directly to the nitrogen atom in a configuration holding the methyl group between and above C*m* and C*m′* (see Fig. 1). Other NOESY correlations can be used to determine the configuration about C*f*. The much more intense *f*–*m*(eq) and *f*–*m′*(eq) correlations relative to *f*–*m*(ax) and *f*–*m′*(ax) for example, demonstrate that the C*f*–H*f* bond occurs at the equatorial position, leaving the C*f*–O bond in the axial position and on the opposite side of the ring system from the methyl group. Finally, a NOESY spectrum of the compound dissolved in $CDCl_3$ (not shown) contained intense correlations between the hydroxyl group ^1H and both H*g* signals, implicating that the hydroxyl group is directly bonded to C*g*.

With the exception of the remaining connectivities for C*j* and C*k*, the structure has been completely elucidated. From the

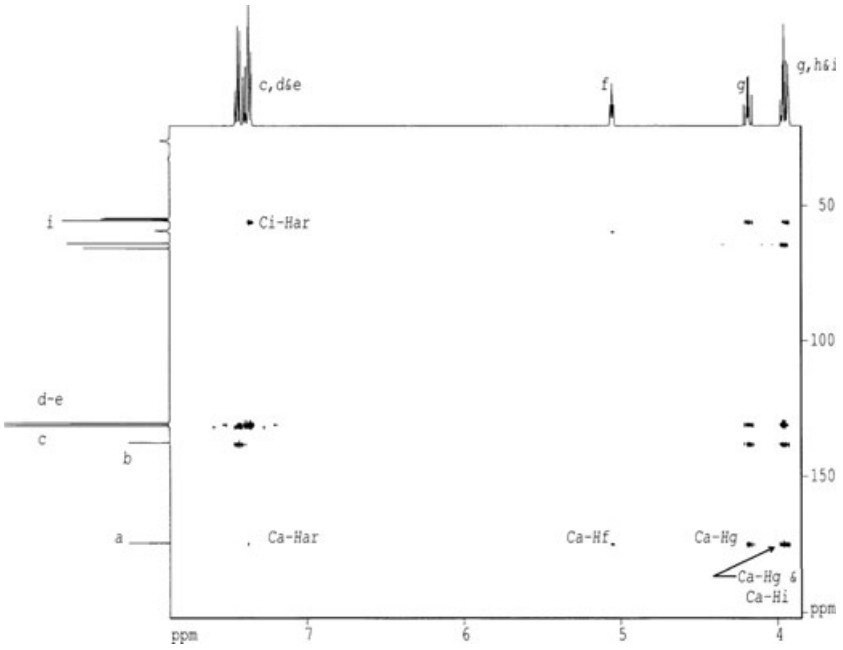

FIG. 6—*^1H–^{13}C heteronuclear multiple bond correlation (HMBC) subspectrum of the unidentified powder dissolved in D_2O, with the corresponding regions of the ^1H and $^{13}C\{^1H\}$ spectra. Long-range correlations demonstrating the connectivities of specific chemical groups in the molecular structure are labeled.*

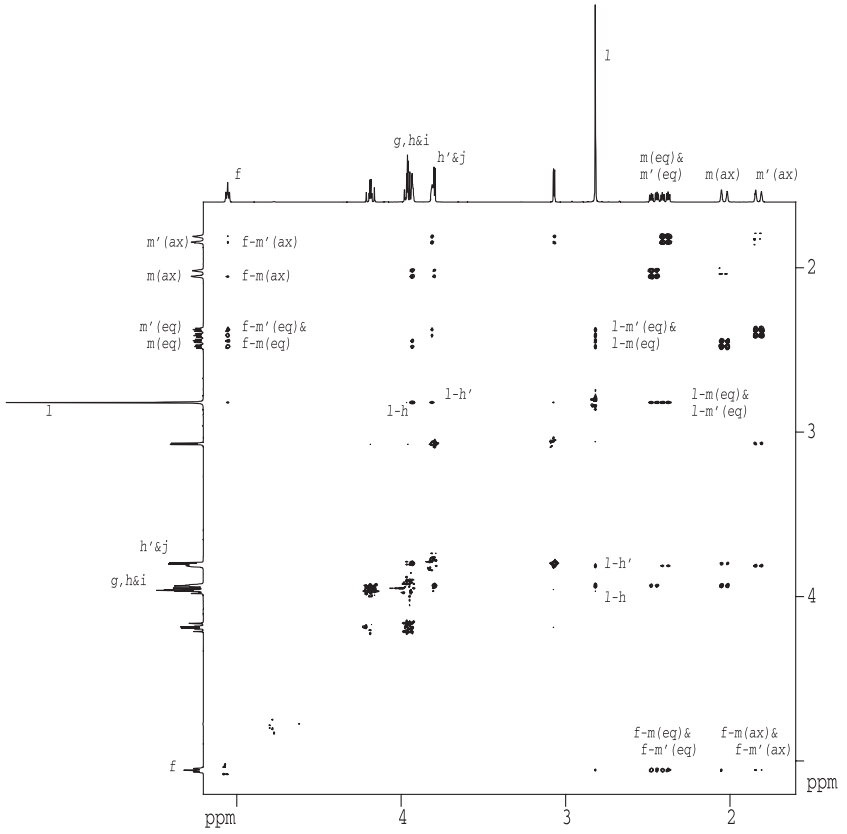

FIG. 7—*Nuclear Overhauser effect spectroscopy (NOESY) subspectrum of the unidentified powder dissolved in D_2O, with the corresponding region of the ^1H spectrum shown for both dimensions. Correlations placing the methyl group in conformational space, and the configuration about carbon atom f, are designated.*

one-dimensional NMR data, it is clear that these connectivities do not involve carbon, nitrogen, phosphorus or fluorine atoms, or other protons. Signals H*j* and H*k* display no evidence of *J*-coupling to NMR-active nuclei other than each other, eliminating any utility for further NMR spectroscopy. At this point, we considered the molecular structures of target analytes to provide clues, and discovered that by simply connecting C*j* and C*k* with a single oxygen atom to create an epoxy group (see Fig. 1), a tropane ring system could be formed to generate the structure of the scopolamine neurotoxin ($C_{17}H_{21}NO_4$, 303.35 g/mole). ^1H and ^{13}C spectroscopy of authentic scopolamine dissolved in D_2O (not shown) validated the sample as scopolamine.

The NMR results were corroborated by ESI^+-MS and ESI^+-MS/MS of a 0.1 mg/mL solution of the unknown powder. As shown in Fig. 8, a clean electrospray mass spectrum with a prominent base signal centered at m/z 304.1 was produced. Additional signals were observed at m/z 305.1 and 306.1, corresponding respectively, to 19 and 3% of the m/z 304.1 ion intensity. Also evident is a low intensity m/z 325.9 signal consistent with the sodium adduct $(M+Na)^+$ of scopolamine. Increases in ionization potential produced corresponding relative increases in m/z 138.1 and 156.1 intensity, and MS/MS also produced major characteristic fragments at m/z 138.1 and 156.1; see Fig. 9.

The prominent m/z 304.1 base signal (Fig. 8) supports the molecular formula $C_{17}H_{21}NO_4$ for the powder's major component, and further, is consistent with the molecular ion $(M+H)^+$ of scopolamine. The isotope pattern observed agrees very favorably with the theoretical values for this formula (19 and 3% observed, compared with the calculated values of 19.7 and 2.6%, respectively).

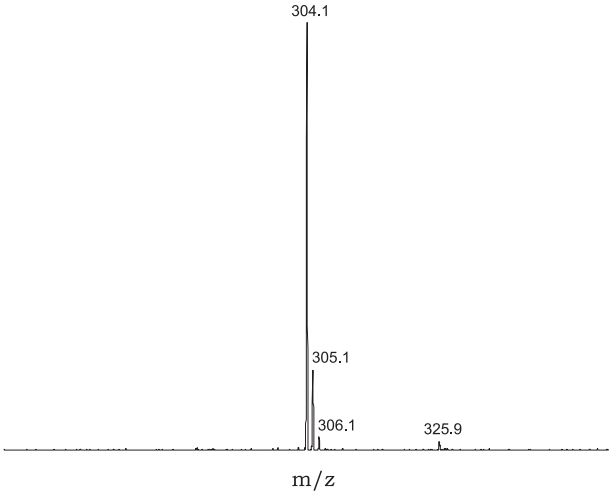

FIG. 8— *Mass spectrum (250–350 amu zoom scan) of the unidentified powder dissolved in 50% ethanol/50% H_2O (v/v).*

In-source fragmentation and MS/MS data support this conclusion as well, and both are consistent with previous reports (23–25). The m/z 156.1 major fragment can be attributed to cleavage of the bond between the carbonyl carbon and the ester oxygen on the tropane ring, with charge retained on the ring to leave a m/z 156 fragment. Likewise, the m/z 138 fragment corresponds to the m/z 156 fragment with a loss of water (23–25).

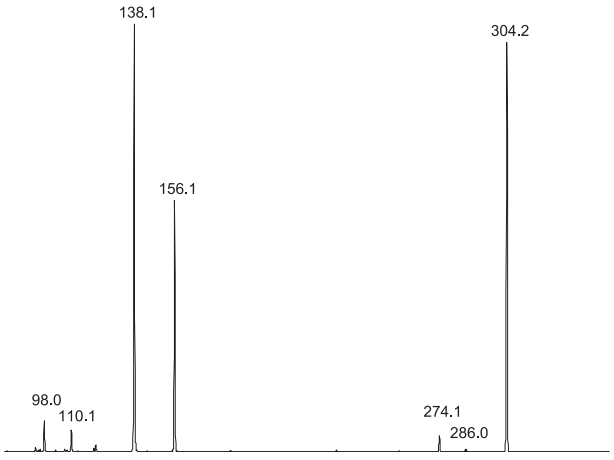

FIG. 9— *ESI⁺-MS/MS spectrum of the unidentified powder base signal, m/z 304.1.*

Comparison of NMR Results to Previously Reported Data

There is a significant number of NMR investigations in the literature addressing scopolamine structure (26–42) that permit direct comparisons between our measured NMR parameters and previously published values. We have made several such comparisons for our chemical shift and $J_{H,H}$ measurements, and have presented them in table form. Table 1 summarizes comparisons of our ^{1}H and ^{13}C chemical shift measurements to previously reported values from three different reports, while Table 2 lists our $J_{H,H}$ measurements for the scopolamine tropane ring protons and those from an earlier report. In both tables, the tropane ring positions used to identify individual carbon atoms (C-1 to C-7) and protons (H-1 to H-7, including all axial, *ax*, and equatorial, *eq*, protons) are illustrated in the bottom panel of Fig. 1.

Our ^{13}C chemical shift measurements agree favorably with previously reported values for scopolamine in D_2O. Table 1 reveals that our ^{13}C chemical shift assignments for the scopolamine tropane ring closely resemble those of Feeney and coworkers (32), who

TABLE 1—*^{13}C and ^{1}H chemical shift values (ppm) for scopolamine in D_2O.*

^{13}C Chemical Shifts (δ)					^{1}H Chemical Shifts (δ)		
		Reference					
^{13}C Site	Current data	(32)	(36)	(42)	^{1}H Site	Current data	Reference (32)
C = O	175.01	*	174.86	175.05	H(*meta*)	7.44	*
C(*ipso*)	138.12	*	138.16	138.28	H(*ortho*)	7.43	*
C(*meta*)	131.85	*	130.85†	131.93	H(*para*)	7.37	*
C(*ortho*)	130.98	*	131.66†	131.04	H-3	5.06	5.05
C(*para*)	130.93	*	130.69	130.99	$-CH_{2a}-$	4.19	*
C-3	66.31	64.68	66.05	66.26	–CH(*Ph*)–	3.97	*
$-CH_2-$	64.49	*	64.57	64.64	$-CH_{2b}-$	3.96	*
C-5	59.52	58.27	59.48	59.65	H-5	3.94	3.94
C-1	59.39	58.13	59.34	59.49	H-1	3.82	3.82
–CH(*Ph*)–	56.01	*	56.06	56.17	H-6	3.80	3.80
C-6	55.48	53.92	55.01	55.52	H-7	3.06	3.07
C-7	55.13	53.57	55.30	55.17	$N-CH_3$	2.82	*
$N-CH_3$	32.72	25.72	32.74	32.83	H-4*ax*	2.47	2.47
C-2	26.22	25.20	26.10‡	26.33	H-2*ax*	2.40	2.40
C-4	26.13	25.20	26.22‡	26.22	H-4*eq*	2.04	2.04
					H-2*eq*	1.82	1.82

*Not determined.
†Assignments reversed in Ref. (36) and corrected in Ref. (42).
‡Assignments reversed in Ref. (36) and corrected in Ref. (42).

TABLE 2—*Tropane ring $J_{H,H}$ (Hz) values for scopolamine in D_2O.*

$J_{H,H}$	Current Data	Reference (32)
$J_{1,2ax}$	1.4	1.3
$J_{1,2eq}$	3.5	4.8
$J_{2ax,2eq}$	17.3	17.3
$J_{2ax,3}$	5.0	3.8*
$J_{2eq,3}$	1.0	1.0*
$J_{1,7}$	0.7	<2.0
$J_{4eq,5}$	3.5	4.8
$J_{5,6}$	1.8	<2.0
$J_{6,7}$	3.5	3.6

*Measurements reversed in Ref. (32) and corrected in Ref. (36).

reported the first ^{13}C chemical shift measurements for the toxin in D_2O. Their assignment of 25.27 ppm for the *N*-methyl group signal, however, differs significantly with our finding of 32.72 ppm for the same signal. This reflects the confusion observed in the earlier literature regarding the ^{13}C chemical shift of this group for the toxin in D_2O (38,39). Glaser *et al.* (36) ultimately resolved this confusion by demonstrating that the *N*-methyl group stereochemistry of tropane alkaloids is strikingly solvent sensitive (see Ref. 39 for a detailed discussion). Our measured ^{13}C chemical shift for this group agrees well not only with that of Glaser *et al.* (36) but also with a later report from the same laboratory (42). Furthermore, all of our ^{13}C chemical shift measurements are remarkably similar to their corresponding values from this latter report (42). Each of our measurements differs by <0.15 ppm from their previously reported value, and most differ by <0.10 ppm.

In contrast to ^{13}C chemical shift data, the literature contains very little information concerning ^{1}H chemical shift measurements for scopolamine in D_2O. Although Feeney *et al.* (32) reported such measurements, these we limited to only the tropane ring proton signals. In general terms, our ^{1}H chemical shift measurements are identical, or essentially identical, to these earlier measurements. As shown more specifically in Table 1, seven of our measurements are identical to their corresponding values appearing in the earlier report, and the remaining two differ from their previously reported values by only 0.01 ppm. The table also lists our ^{1}H chemical shift measurements for the remaining scopolamine protons. Corresponding values for these protons are reported for scopolamine in CD_2Cl_2 (36) and $CDCl_3$ (35,38); however, we hesitate to make comparisons of chemical shift values derived from different solvents, as solvent effects can significantly impact chemical shift values. The H-4*ax* signal for example, is found at 2.47 ppm from our measurements (see Table 1) and others (32) for the toxin in D_2O, but appears at 3.31 and 2.08 ppm for the toxin in CD_2Cl_2 (36) and $CDCl_3$ (38), respectively. Such differences can appear discordant without detailed explanations, and offer little when attempting to corroborate different sets of data.

As for the ^{1}H chemical shift data, Feeney *et al.* (32) report the only $J_{H,H}$ measurements for scopolamine in D_2O, and these are, again, confined to only the tropane ring protons. We have listed these measurements and our own in Table 2 for direct comparison. In general, the two sets of measurements are in good agreement with each other. Of the nine pairs of corresponding values listed in the table, only two, $J_{1,2eq}$ and $J_{4eq,5}$, appear to possibly reflect minor disparities. It is not clear whether these differences result from measurement errors or differences in tropane ring conformation.

Finally, Sarazin *et al.* (38) reported results from a $^{1}H–^{1}H$ chemical shift correlation and a long-range, $^{1}H–^{13}C$ chemical shift

correlation for scopolamine in $CDCl_3$, experiments which are analogous to our COSY (Fig. 5) and HMBC (Fig. 6) experiments, respectively. In large part, our spectra resemble those from this earlier report, even though they were conducted with the toxin in D_2O. Most importantly, all correlations identified by our experiments appear to have a corresponding correlation in the earlier reported spectra. Some significant differences are apparent on the other hand, which give our spectra somewhat of a different appearance. The most striking difference is that our spectra have considerably more resolution, a consequence of our use of a higher magnetic field strength (the earlier data was recorded at 7.06 Tesla), and in the case of our COSY experiment, the use of phase sensitive pulse sequences rather than those generating magnitude spectra. Another major source leading to spectral differences is the disparity in chemical shift values of the scopolamine protons for the two solvents. This is particularly the case for H-1, H-5 and H-6, which appear between 3.80 and 3.94 ppm in D_2O (see Table 1), but between 2.94 and 3.37 ppm in $CDCl_3$, placing correlations involving these protons in different regions of our COSY and HMBC spectra relative to their respective, previously published spectra. Although comparisons to chemical shift correlation spectra for scopolamine in D_2O would have been more appropriate, no such spectra appear in the literature.

Conclusions

We have used several NMR techniques to characterize an unidentified white powder seized in an intelligence investigation. Collectively, the techniques were able to give a good estimate of the specific types and number of different atoms comprising the principal component of the powder, and essentially all of the information necessary to determine its chemical structure. This structure was easily elucidated, positively identifying the principal component as scopolamine. This investigation is just one example of an ever increasing number of forensic investigations involving biotoxins in crimes and acts of terror. In recent years, technical information relating to biochemical weapons has become readily accessible on the internet, and today, many of the materials for their isolation and purification are available for legitimate commercial purposes. The capability of hostile nations and terrorist groups for acquiring these weapons is greater now than at any other time in history. For these reasons, the analysis of law enforcement and intelligence samples for biological toxins has never been more important. Although more routine techniques relying on spectral libraries and other analytical data such as chromatographic retention times can be rapid and effective, they do not always lead to a positive identification of biological toxins. This is particularly the case for larger protein toxins such as ricin, staphylococcal enterotoxins and botulinum neurotoxins, where reliable detection can be a formidable challenge. Further, impurities that are valuable in determining which government, country or terrorist group has purified or supplied the weapon usually do not appear in spectral libraries. And there is an ever increasing likelihood of encountering unique toxins which are evolutionarily related to the more commonly known toxins (at least five evolutionarily related tetrodotoxins have been identified for example, see Refs. 43 and 44), chemically modified nonprotein toxins, or even emerging threat agents such as genetically engineered protein toxins (45–50). In such cases, the elucidation of analyte molecular structure by interpretative means may present the best, and sometimes only, means for identification. While several techniques can provide valuable information for determining molecular structure, NMR spectroscopy remains one of the single most powerful techniques for providing detailed and unambiguous structural information within a reasonable timeframe. Moreover, both the quantity and quality of structural data deriving from NMR experiments has been expanded considerably with the intense development of multi-dimensional techniques over the last 25 years, making NMR spectroscopy indispensable in forensic science today.

References

1. Eggen D. Letter with ricin vial sent to White House. The Washington Post, 2004 Feb 4, Sect. A:7.
2. Fox B. Ricin found in jars of baby food in California. The Washington Post, 2004 Jul 28, Sect. A:6.
3. Uniting and Strengthening America by Providing Appropriate Tools Required to Intercept and Obstruct Terrorism (USA PATRIOT ACT) Act of 2001: House Resolution 3162. 107th Congress, 1st Session, 2001, 24 October, Washington, DC.
4. Bates RG. Determination of pH: theory and practice. New York: John Wiley and Sons, Inc., 1964.
5. Farrar TC, Becker ED. Pulse and Fourier transform NMR. New York: Academic Press, 1967.
6. Opella SJ, Nelson DJ, Jardetzky O. ^{13}C nuclear magnetic resonance study of molecular motions and conformational transitions in muscle calcium binding parvalbumins. J Chem Phys 1976;64:2533–5.
7. Shaka AJ, Keeler J, Freeman R. Evaluation of a new broadband decoupling sequence: WALTZ-16. J Magn Reson 1983;53:313–40.
8. Henderson TJ. Sensitivity-enhanced quantitative ^{13}C NMR spectroscopy via cancellation of $^{1}J_{CH}$ dependence in DEPT polarization transfers. J Am Chem Soc 2004;126:3682–3.
9. Redfield AG, Kunz SD. Quadrature Fourier NMR detection: simple multiplex for dual detection and discussion. J Magn Reson 1975;19:250–4.
10. Jeener J, Meier BH, Bachmann P, Ernst RR. Investigation of exchange processes by two-dimensional NMR spectroscopy. J Chem Phys 1979;71:4546–53.
11. Wagner R, Berger S. Gradient-selected NOESY—a fourfold reduction of the measurement time for the NOESY experiment. J Magn Reson Series A 1996;123:119–21.
12. States DJ, Haberkorn RA, Ruben DJ. A two-dimensional nuclear Overhauser experiment with pure absorption phase in four quadrants. J Magn Reson 1982;48:286–92.
13. Gesmar H, Led JJ. Spectral estimation of two-dimensional NMR signals by applying linear prediction to both dimensions. J Magn Reson 1988;76:575–86.
14. Zeng Y, Tang J, Bush CA, Norris JR. Enhanced spectral resolution in 2D NMR signal analysis using linear prediction extrapolation and apodization. J Magn Reson 1989;83:473–83.
15. Olejniczak ET, Eaton HL. Extrapolation of time-domain data with linear prediction increases resolution and sensitivity. J Magn Reson 1990;87:628–32.
16. Palmer AG, III. Cavanaugh J, Wright PE, Rance M. Sensitivity improvement in proton-detected two-dimensional heteronuclear correlation NMR spectroscopy. J Magn Reson 1991;93:151–70.
17. Kay LE, Keifer P, Saarinen T. Pure absorption gradient enhanced heteronuclear single quantum correlation spectroscopy with improved sensitivity. J Am Chem Soc 1992;114:10663–5.
18. Schleucher J, Schwendinger M, Sattler M, Schmidt P, Schedletzky O, Glazer SJ, Sorensen OW, Griesinger C. A general enhancement scheme in heteronuclear multidimensional NMR employing pulsed field gradients. J Biomol NMR, 1994;4:301–6.
19. Hurd RE, Boban JK. Gradient-enhanced proton-detected heteronuclear multiple quantum coherence spectroscopy. J Magn Reson 1991;91:648–53.
20. Gibbs SJ, Johnson CS Jr. A PFG NMR experiment for accurate diffusion and flow studies in the presence of eddy currents. J Magn Reson 1991;93:395–402.
21. Silverstein RM, Bassler GC, Morrill TC. Spectrometric identification of organic compounds, 5th ed. New York: John Wiley and Sons, Inc., 1991.
22. Aydin R, Loux J-P, Günther H. Karplus curve for $^{3}J(^{13}C, ^{1}H)$ in hydrocarbons. Agnew Chem (Internat) 1982;21:499.
23. Kintz P, Villain M, Barguil Y, Charlot JY, Cirimele V. Testing for atropine and scopolamine in hair by LC-MS-MS after Datura intoxia abuse. J Anal Tox 2006;30:454–7.
24. Oertel R, Richter K, Ebert U, Kirch W. Determination of scopolamine in human serum and microdialysis samples by liquid chromatography-

tandem mass spectrometry. J Chromatogr B Biomed Sci Appl 2001;750:121–8.
25. Beyer J, Peters FT, Kramer T, Maurer HH. Detection and validated quantification of toxic alkaloids in human blood plasma - comparison of LC-APCI-MS with LC-ESI-MS/MS. J Mass Spectrom 2007;42:621–33.
26. Johns SR, Lamberton JA. Magnetic non-equivalence of the epoxide ring (C-6 and C-7) protons of scopolamine. J Chem Soc, Chem Commun 1965:458–9.
27. Mandava N, Fodor G. Configuration of the ring nitrogen in *N*-oxides and the conformation of tropanes. Part XVIII. Can J Chem 1968;46:2761–6.
28. Wenkert E, Bindra JS, Chang C-J, Cochran DW, Schell FM. Carbon-13 nuclear magnetic resonance spectroscopy of naturally occurring substances. Alkaloids. Acc Chem Res 1974;7:46–51.
29. Simeral L, Maciel GE. Carbon-13 chemical shifts of some cholinergic neural transmission agents. Org Magn Reson 1974;6:226–32.
30. Leete E, Kowanko N, Newmark RA. Use of carbon-13 nuclear magnetic resonance to establish that the biosynthesis of tropic acid involves an intramolecular rearrangement of phenylalanine. J Am Chem Soc 1975;97:6826–30.
31. Hanisch P, Jones AJ, Casey AF, Coates JE. Carbon-13 magnetic resonance: evidence for non-chair conformations in tropane derivatives. J Chem Soc Perkin Trans 2 1976:1202–8.
32. Feeney J, Foster R, Piper EA. Nuclear magnetic resonance study of the conformations of atropine and scopolamine cations in aqueous solution. J Chem Soc Perkin Trans 2 1977:2016–20.
33. Taha AM, Rücher G. ^{13}C-NMR spectroscopy of tropane alkaloids. J Pharm Sci 1978;67:775–9.
34. Mislow K, Siegel J. Stereoisomerism and local chirality. J Am Chem Soc 1984;106:3319–28.
35. Chazin WJ, Colebrook LD. Use of spin-lattice relaxation and nuclear Overhauser effect data in structure analysis of alkaloids. J Org Chem 1986;51:1243–53.
36. Glaser R, Peng Q-J, Perlin AS. Stereochemistry of the *N*-methyl group in salts of tropane alkaloids. J Org Chem 1988;53:2172–80.
37. Glaser R, Charland J-P, Michel A. Solid-state stereochemistry of anhydrous (−)-scopolamine hydrobromide. J Chem Soc Perkin Trans 2 1989:1875–89.
38. Sarazin C, Goethals G, Séguin J-P, Barbotin J-N. Spectral reassignment and structure elucidation of scopolamine free base through two-dimensional NMR techniques. Magn Reson Chem 1991;29:291–300.
39. Glaser R. NMR and molecular mechanics studies on the solution-state conformation of (−)-scopolamine free base. Magn Reson Chem 1993;31:335–9.
40. Michel A, Drouin M, Glaser R. Solid-state stereochemistry of (−)-scopolamine hydrobromide sesquihydrate, a new polymorph of the cholinergic drug. J Pharm Sci 1994;83:508–13.
41. Naqui AA, Mandal S, Verma RK. Determination of atropine and scopolamine by proton nuclear magnetic resonance spectroscopy. Phytochem Anal 1998;9:168–70.
42. Glaser R, Shiftan D, Drouin M. Conformational psuedopolymorphism and solid-state CPMAS NMR studies for determination of solvent-dependent solution-state conformational preferences for (-)-scopolamine hydrobromide/hydrochloride salts. J Org Chem 1999;64:9217–24.
43. Nakamura M, Yasumoto T. Tetrodotoxin derivatives in puffer fish. Toxicon 1985;23:271–6.
44. Yotsu-Yamashita M, Schimmele B, Yasumoto T. Isolation and structural assignment of 5-deoxytetrodotoxin from the puffer fish *fufu poecilonotus*. Biosci Biotechnol Biochem 1999;63:961–3.
45. Kondo T, Kurihara S, Yoshikawa T, Mizukami H. Effect of N- and C-terminal deletions on the RNA *N*-glycosidase activity and the antigenicity of karasurin-A, a ribosome inactivating protein from *Trichosanthes kirilowii* var. japonica. Biotechnol Lett 2004;26:1873–8.
46. He WJ, Liu WY. Both N- and C-terminal regions are essential for cinnamomin A-chain to deadenylate ribosomal RNA and supercoiled double stranded DNA. Biochem J 2004;377:17–23.
47. Herrero S, Gonzalez-Cabrera J, Ferre J, Bakker PL, de Maagd RA. Mutations in the *Bacillus thuringiensis* Cry1catoxin demonstrate the role of domains II and III in specificity towards *Spodoptera exigua* larvae. Biochem J 2004;384:507–13.
48. Dai Q, Castellino FJ, Prorok M. A single amino acid replacement results in the Ca^{2+}-induced self assembly of a helical conantokin-based peptide. Biochemistry 2004;43:13225–32.
49. Clark RJ, Fischer H, Dempster L, Daly NL, Rosengren KJ, Nevin ST, Maunier FA, Adams DJ, Craik DJ. Engineering stable peptide toxins by means of backbone cyclization: stabilization of the alpha-conotoxin MII. Proc Natl Acad Sci U S A 2005;102:13767–72.
50. Morinaga N, Yahiro K, Matsurra G, Watanabe M, Nomura F, Moss J, Noda M. Two distinct cytotoxic acitvities of subtilase cytotoxin produced by shiga-toxingenic *Escherichia coli*. Infect Immun 2007;75:488–96.

Additional information and reprint requests:
Terry J. Henderson, Ph. D.
Research Chemist
Edgewood Chemical Biological Center
AMSRD-ECB-RT-CF
5183 Blackhawk Road
Aberdeen Proving Ground, MD 21010-5424
E-mail: terry.j.henderson@us.army.mil